journal

J. Am. Ceram. Soc., 1–7 (2012)
DOI: 10.1111/j.1551-2916.2012.05415.x
© 2012 The American Ceramic Society

Understanding the Crystallization Mechanism of a Wollastonite Base Glass Using Isoconversional, IKP Methods and Master Plots

Juan M. Pérez,[‡] Silvio R. Teixeira,[§] Jesús Ma. Rincón,[‡] and Maximina Romero[‡,†]

[‡]Group of Glassy and Ceramic Materials, Instituto de Ciencias de la Construcción Eduardo Torroja, CSIC, Madrid 28033, Spain

[§]Departamento Fisica, Quimica e Biologia, Universidade Estadual Paulista-UNESP, Presidente Prudente, São Paulo 19060-080, Brazil

The complex development of crystals found in the crystallization of SiO_2–Al_2O_3–CaO–Na_2O glass has been explained using Differential Thermal Analysis. The crystal growth process has been studied using isoconversional, invariant kinetic parameters, and master plots methods. The applied kinetic models have revealed activation energy values that are over 360 and 385 kJ/mol by employing the integral and differential kinetic methods, respectively. The crystallization process schedule that was previously observed using scanning electron microscopy has been corroborated in this study using the kinetic methods. The crystallization of wollastonite occurs through a complex two-stage mechanism, with early three-dimensional growth of crystals (A_3 mechanism) on the surface of glass particles followed by one-dimensional growth of needles ($A_{3/2}$ mechanism) toward the interior of grains. The results presented in this article are in agreement with a previous paper that employed the Kissinger non-isothermal method and the Ligero approximation.

I. Introduction

GLASS-CERAMICS are materials that contain small crystals embedded in a glassy matrix. The key to improving and controlling the final properties of these materials lies in the shape of and the way these crystals are developed in the parent glass. The most common way to produce a glass-ceramic is through a controlled crystallization process that involves two steps: nucleation and crystal growth. In the former, small nuclei are developed on the surface and/or in the bulk glass; and in the latter, these nuclei, or small crystals, grow to a suitable size.

The SiO_2–Al_2O_3–CaO system is one of the most known and studied for glass-ceramics production,[1] as base glasses of this system are suitable for producing glass-ceramics with wollastonite ($CaO{\cdot}SiO_2$) as the main crystalline phase, according to a mechanism of controlled surface crystallization. At temperatures above 950°C, base glasses of this system exhibit the crystallization of β–wollastonite on the surface, and at 1000°C, wollastonite begins to grow as needles from the edge to the interior of the bulk glass. If the temperature rises to 1180°C, spherical crystals of β–wollastonite can also be formed.

Wollastonite is the main crystalline phase of the commercial material known as Neoparies®, which is manufactured from pure raw materials. This material is the first glass-ceramic employed as construction material in building applications. The main characteristics of glass-ceramic materials include their wide range of compositions and the possibility of developing heterogeneous microstructures, which implies a lack of restriction in the amount of oxides that can be incorporated. This feature affords the possibility of using the glass-ceramic process for wastes valorization. In fact, the flexibility of this process is evidenced by the variety of mineral or industrial wastes that have been used as raw materials for the production of glass-ceramics,[2,3] and these wastes include fly ashes from incineration[4,5] and thermal power plants,[6] wastes from hydrometallurgical processing plants,[7] fiberglass wastes from polyester matrix composites,[8] and rice husk ash.[9] An advantage of including wastes in the production of glass-ceramic materials is the lower cost compared to using pure, raw materials. Moreover, wastes usually content in their chemical composition minor components, which when incorporated into a glassy network can act as nucleating agents favouring the crystallization process.[10,11]

Previously, Teixeira *et al.*[12] have shown that a wollastonite glass-ceramic, similar to Neoparies®, could be prepared using sugarcane bagasse ash as a silica source, thereby demonstrating the possibility of using waste valorization to develop suitable final properties for the industrial construction sector. They concluded that the crystallization of wollastonite occurs through a complex mechanism during heating. The results obtained by differential thermal analysis (DTA) indicated that bi-directional surface crystallization is the main route for glass devitrification. However, the kinetic study concluded that bulk crystallization occurs through the three-dimensional growth of crystals and is the principal mechanism for wollastonite formation. Finally, scanning electron microscopy micrographs revealed that both processes occur simultaneously, i.e., crystallization began with the early surface crystallization of three-dimensional crystals that were subsequently transformed into needles (one-dimensional growth). The incomplete information obtained from the kinetic methods used in the former paper requires the need for a wider kinetic study that employs complex models that could explain the coexistence of both surface and bulk mechanisms during a single crystallization process.

The most commonly used methods for the kinetic analysis of solid-state reactions are the non-isothermal methods. There are several ways to study reactions under non-isothermal conditions. The activation energy is generally determined as a function of the reacted fraction, without using any previous assumptions in the kinetic model fitted to the reaction, by using isoconversional methods. Isokinetic methods assume that the transformation mechanism is the same throughout the temperature and time range of interest and that the kinetic parameters are supposed to be constant with respect to time and temperature. Master plots are well-known theoretical curves that depend on the reaction model and are

L. Pinckney—contributing editor

Manuscript No. 31275. Received March 30, 2012; approved July 18, 2012.
[†]Author to whom correspondence should be addressed. e-mail: mromero@ietcc.csic.es

independent of the Arrhenius parameters. The appropriate reaction model can be selected by comparison the experimental and theoretical master plots.

The Isokinetic Relationship (IKR) and Invariant Kinetic Parameters (IKP) methods have been widely applied to the study of the decomposition of aromatic azomonoethers,[13] polymer curing,[14] polymerization of poly(ester amide) potassium salt[15] nickel oxide reduction study,[16] and even to crystallization of silica-soda-lead glass[17] and mullite development.[18]

The aim of the present work is to determine the kinetics parameters for the crystallization process of a wollastonite base glass. During this study, the isoconversional (integral and differential methods), IKR, and IKP methods were utilized. The experimental data were fit to integral and differential master plots, and finally, the present results are compared with those that were previously obtained using the Kissinger and Ligero methods.[12]

II. Experimental Procedure

(1) Materials and Methods

The wollastonite base glass studied here belongs to the SiO_2–Al_2O_3–CaO–Na_2O system, and its preparation and chemical composition have been described by Teixeira *et al.*[12]

Differential thermal analysis was performed using a SETARAM Labsys Thermal Analyzer. The samples were analyzed in platinum crucibles with calcined Al_2O_3 as a reference material from room temperature to 1523 K at heating rates of 5, 10, 20, 30, 40, and 50 K/min. The obtained data were analyzed using the Friedman[19] and Kissinger–Akahira–Sunose[20,21] isoconversional methods; the IKR, IKP, and the integral and differential master plots as it is described below.

(2) Kinetic Methods

(A) Isoconversional Methods: The employed isoconversional methods are based on dynamic DTA. The equation for the reaction rate used to study the degree of crystallization can generally be expressed as:

$$\frac{d\alpha}{dt} = k(T)\cdot f(\alpha) \tag{1}$$

where α is the extent of the reaction, $k(T)$ is the rate constant expressed by the temperature-dependent Arrhenius equation and $f(\alpha)$ is the reaction model function. Taking into account that under non-isothermal conditions, $d\alpha/dt = \beta\,(d\alpha/dT)$, where β is the heating rate (K/min), Eq. (1) can be rewritten as:

$$\beta\cdot\frac{d\alpha}{dT} = A\cdot e^{-E_a/R\cdot T}\cdot f(\alpha) \tag{2}$$

where T is the temperature, A is the pre-exponential factor, R is the gas constant, and E_a is the activation energy, which is independent of conversion.

By taking the logarithm of each side of Eq. (2), the Friedman differential isoconversional method is obtained as follows:

$$\ln\left(\frac{d\alpha}{dt}\right) = \ln[A\cdot f(\alpha)] - \frac{E_a}{R\cdot T} \tag{3}$$

and the rate equation can be expressed in its integral form as:

$$g(\alpha) = \int_0^{\alpha}\frac{d\alpha}{f(\alpha)} = \frac{A}{\beta}\int_0^{T} e^{(-E_a/R\cdot T)}dT \tag{4}$$

Assuming that the p-Doyle function,[22] $p(E_a/RT)$, can be expressed using the Murray and White approximation,[23] the Kissinger–Akahira–Sunose (KAS) model-free method can be originally obtained by applying the following equation:

$$\ln\left(\frac{\beta}{T^2}\right) = \ln\left(\frac{R\cdot A}{E_a\cdot g(\alpha)}\right) - \frac{E_a}{R}\cdot\frac{1}{T} \tag{5}$$

In this case, the method does not require knowledge of the conversion-dependent functions ($f(\alpha)$ or $g(\alpha)$), and the only assumption is that the process follows the same reaction mechanism for a given degree of conversion, regardless of the crystallization temperature.

(B) Model Fitting Methods: These methods obtain the kinetic parameters with a single heating rate. In this work, the methods that have been employed are as follows:

-the integral method, known as the Coats–Redfern (C–R) method[24]:

$$\ln\left[\frac{g(\alpha)}{T^2}\right] = \ln\left[\frac{A\cdot R}{\beta\cdot E_a}\right] - \frac{E_a}{R\cdot T} \tag{6}$$

-the differential method (D), which is based on Eq. (3):

$$\ln\left[\frac{d\alpha/dt}{f(\alpha)}\right] = \ln A - \frac{E_a}{R\cdot T} \tag{7}$$

For a given model (see Table I in Ref. 18) and heating rate, the linear plot of the left-hand sides vs T^{-1} permitted the determination of E_a and A from the slope and the intercept, respectively.

(C) Compensation Effect: The activation energy and the pre-exponential factor may be combined due to the so-called compensation effect or IKR through[25,26]:

$$\ln A_x = \alpha^* + \beta^* E_x \tag{8}$$

where α^* and β^* are constants and the subscripts, x, refer to a factor that produces a change in the Arrhenius parameters (conversion, heating rate and model). The intercept, $\alpha^* = \ln k_{iso}$, is related to the isokinetic rate constant (k_{iso}), and the slope, $\beta^* = 1/RT_{iso}$, is related to the isokinetic temperature (T_{iso}). The appearance of the IKR indicates that only one mechanism is present, whereas the existence of parameters that do not agree with the IKR implies that there are multiple reaction mechanisms.[26]

According to certain authors,[25] we may select the model whose IKR, in relation to the conversion, has the best linear correlation and in which the associated T_{iso} value was near the experimental temperature range.

(D) Invariant Kinetic Parameters Method: The IKP method[27,28] is based on the observation that the experimental curve, $\alpha(T)$, could be approximately correct when described by several conversion functions. By using the apparent compensatory effect that exists when the model changes for each heating rate (β_v, v = 1, 2, 3…), the compensation parameters, α_v^* and β_v^*, are determined according to Eq. (8). A set of conversion functions, f_j, where j = 1, 2, 3…, are also considered (Table I in Ref. 18). For each heating rate, β_v and the pairs (A_{vj}, E_{vj}) that are characteristic of each conversion are determined using an integral or differential method. In this work, the integral method suggested by C–R [Eq. (6)] and the differential method based on Eq. (7) will be used.

A plot of each of these equations should be a straight line formed from ln ($AR/\beta E_a$) or ln A respectively, and ($-E_a/R$).

Using the apparent compensation effect relationship, the compensation parameters (α^*_v, β^*_v) are determined for each heating rate. The intersection point of the straight lines corresponds to the true values of A and E. These were called the invariant parameters (A_{inv}, E_{ainv}) by Lesnikovich and

Table I. Integral Parameters Determined by Using C–R [Eq. (6)] Method

	Heating rate								
	β = 5°C/min			β = 10°C/min			β = 20°C/min		
Model	E_a (kJ/mol)	ln A (s^{-1})	r^2	E_a (kJ/mol)	ln A (s^{-1})	r^2	E_a (kJ/mol)	ln A (s^{-1})	r^2
$A_{3/2}$	451.05 ± 5.26	47.94 ± 9.33	0.9847	505.48 ± 8.54	53.87 ± 10.16	0.9723	448.68 ± 7.63	47.32 ± 9.94	0.9670
A_2	333.75 ± 3.95	34.78 ± 8.90	0.9843	374.51 ± 6.40	39.43 ± 9.64	0.9716	331.81 ± 5.72	34.65 ± 9.45	0.9661
A_3	216.46 ± 2.64	21.50 ± 8.35	0.9834	243.53 ± 4.27	24.86 ± 9.01	0.9701	214.95 ± 3.82	21.84 ± 8.84	0.9641
A_4	157.81 ± 1.98	14.75 ± 7.99	0.9824	178.04 ± 3.21	17.47 ± 8.61	0.9686	156.52 ± 2.87	15.34 ± 8.45	0.9619
R_1	488.15 ± 10.21	51.60 ± 10.54	0.9524	540.22 ± 14.68	57.21 ± 11.37	0.9312	479.85 ± 12.71	50.21 ± 10.99	0.9235
R_2	579.46 ± 9.31	61.31 ± 10.35	0.9714	645.01 ± 14.02	68.24 ± 11.26	0.9548	573.27 ± 12.30	59.81 ± 10.91	0.9485
R_3	613.17 ± 8.90	64.74 ± 10.26	0.9766	683.82 ± 13.68	72.16 ± 11.19	0.9615	607.87 ± 12.06	63.21 ± 10.87	0.9556
D_1	994.42 ± 20.42	107.31 ± 12.36	0.9541	1098.87 ± 29.35	117.76 ± 13.66	0.9334	978.49 ± 25.41	103.22 ± 13.03	0.9262
D_2	1107.50 ± 19.51	119.41 ± 12.21	0.9658	1228.32 ± 28.79	131.45 ± 13.58	0.9479	1093.88 ± 25.10	115.15 ± 12.99	0.9415
D_3	1244.47 ± 17.78	133.36 ± 11.93	0.9772	1386.07 ± 27.36	147.44 ± 13.37	0.9625	1234.52 ± 24.12	128.99 ± 12.84	0.9569
D_4	1152.80 ± 18.95	123.02 ± 12.12	0.9701	1280.47 ± 28.33	135.73 ± 13.51	0.9533	1140.37 ± 24.79	118.72 ± 12.94	0.9472
F_1	685.64 ± 7.89	74.06 ± 10.03	0.9851	767.44 ± 12.80	82.58 ± 11.03	0.9729	682.41 ± 11.44	72.49 ± 10.75	0.9679
F_2	437.02 ± 6.81	47.43 ± 9.76	0.9731	507.44 ± 6.11	55.16 ± 9.57	0.9857	450.07 ± 4.44	48.55 ± 9.06	0.9886
F_3	892.18 ± 13.62	99.09 ± 11.21	0.9741	1033.30 ± 12.23	113.74 ± 10.92	0.9862	918.91 ± 8.89	99.98 ± 10.22	0.9891

	β = 30°C/min			β = 40°C/min			β = 50°C/min		
Model	E_a (kJ/mol)	ln A (s^{-1})	r^2	E_a (kJ/mol)	ln A (s^{-1})	r^2	E_a (kJ/mol)	ln A (s^{-1})	r^2
$A_{3/2}$	495.08 ± 9.44	52.38 ± 10.34	0.9646	497.46 ± 9.78	52.48 ± 10.40	0.9638	487.04 ± 9.40	51.14 ± 10.31	0.96134
A_2	366.58 ± 7.08	38.56 ± 9.80	0.9636	368.32 ± 7.34	38.71 ± 9.86	0.9629	360.47 ± 7.05	37.75 ± 9.78	0.96033
A_3	238.08 ± 4.72	24.62 ± 9.14	0.9617	239.19 ± 4.90	24.81 ± 9.19	0.9609	233.90 ± 4.70	24.23 ± 9.13	0.95817
A_4	173.83 ± 3.54	17.55 ± 8.73	0.9597	174.62 ± 3.67	17.76 ± 8.78	0.9588	170.61 ± 3.53	17.37 ± 8.72	0.95584
R_1	525.90 ± 15.47	55.19 ± 11.47	0.9195	527.88 ± 16.01	55.22 ± 11.54	0.9180	517.32 ± 15.20	53.84 ± 11.39	0.9146
R_2	630.10 ± 15.08	65.87 ± 11.40	0.9453	632.79 ± 15.61	65.89 ± 11.48	0.9442	619.98 ± 14.89	64.18 ± 11.34	0.94132
R_3	668.74 ± 14.83	69.67 ± 11.36	0.9527	671.72 ± 15.36	69.68 ± 11.43	0.9517	658.05 ± 14.68	67.85 ± 11.30	0.94897
D_1	1070.73 ± 30.94	112.71 ± 13.79	0.9222	1074.84 ± 32.02	112.50 ± 13.92	0.9207	1053.88 ± 30.40	109.55 ± 13.67	0.91747
D_2	1199.31 ± 30.69	125.95 ± 13.76	0.9379	1204.24 ± 31.78	125.71 ± 13.88	0.9367	1180.55 ± 30.25	122.36 ± 13.65	0.93376
D_3	1356.41 ± 29.65	141.42 ± 13.62	0.9539	1362.53 ± 30.72	141.18 ± 13.74	0.9530	1335.35 ± 29.35	137.32 ± 13.52	0.95038
D_4	1251.23 ± 30.36	130.06 ± 13.71	0.9438	1256.56 ± 31.44	129.82 ± 13.84	0.9427	1231.71 ± 29.97	126.30 ± 13.61	0.93988
F_1	752.08 ± 14.16	79.82 ± 11.24	0.9654	755.72 ± 14.67	79.84 ± 11.32	0.9647	740.19 ± 14.09	77.73 ± 11.20	0.96232
F_2	505.53 ± 4.88	54.57 ± 9.19	0.9907	509.65 ± 5.01	54.86 ± 9.23	0.9907	497.62 ± 4.32	53.33 ± 9.00	0.99193
F_3	1029.98 ± 9.77	111.52 ± 10.40	0.9910	1038.38 ± 10.03	111.80 ± 10.45	0.9910	1014.48 ± 8.65	108.57 ± 10.15	0.99222

Table II. Integral Parameters Determined by Using the Differential [Eq. (7)] Method

	Heating rate								
	β = 5°C/min			β = 10°C/min			β = 20°C/min		
Model	E_a (kJ/mol)	ln A (s^{-1})	r^2	E_a (kJ/mol)	ln A (s^{-1})	r^2	E_a (kJ/mol)	ln A (s^{-1})	r^2
$A_{3/2}$	538.92 ± 6.52	53.84 ± 0.73	0.9864	559.78 ± 12.20	56.04 ± 1.34	0.9678	1086.46 ± 54.22	113.95 ± 5.91	0.9639
A_2	387.36 ± 6.25	36.89 ± 0.70	0.9761	357.91 ± 10.78	33.86 ± 1.18	0.9402	416.07 ± 11.21	39.96 ± 1.21	0.9419
A_3	235.81 ± 5.98	19.83 ± 0.67	0.9430	156.05 ± 9.38	11.56 ± 1.03	0.7976	240.80 ± 10.67	20.92 ± 1.15	0.8567
A_4	160.03 ± 5.84	11.21 ± 0.65	0.8886	55.12 ± 8.68	0.33 ± 0.95	0.3597	153.16 ± 10.40	11.31 ± 1.12	0.7174
R_1	651.48 ± 12.64	66.03 ± 1.41	0.9658	698.96 ± 22.72	70.94 ± 2.49	0.9311	715.93 ± 19.51	71.95 ± 2.11	0.9406
R_2	746.76 ± 9.83	76.11 ± 1.11	0.9840	831.23 ± 18.87	84.89 ± 2.07	0.9652	828.91 ± 16.15	83.57 ± 1.74	0.9688
R_3	778.51 ± 8.90	79.29 ± 0.99	0.9879	875.32 ± 17.59	89.37 ± 1.93	0.9725	866.57 ± 15.04	87.27 ± 1.62	0.9751
D_1	1469.88 ± 16.81	156.41 ± 1.88	0.9878	1784.10 ± 34.80	189.03 ± 3.82	0.9741	1659.87 ± 25.73	172.75 ± 2.78	0.9800
D_2	1560.81 ± 14.24	166.00 ± 1.59	0.9922	1910.13 ± 31.31	202.29 ± 3.44	0.9815	1767.57 ± 22.69	183.80 ± 2.45	0.9862
D_3	1656.57 ± 11.43	175.32 ± 1.28	0.9955	2043.10 ± 27.41	215.51 ± 3.01	0.9876	1881.14 ± 19.34	194.68 ± 2.09	0.9911
D_4	1593.05 ± 13.28	168.14 ± 1.49	0.9935	1954.92 ± 29.98	205.75 ± 3.29	0.9838	1805.82 ± 21.55	186.47 ± 2.33	0.9880
F_1	842.03 ± 7.07	87.57 ± 0.79	0.9934	963.50 ± 15.03	100.23 ± 1.65	0.9832	941.89 ± 12.83	96.58 ± 1.38	0.9845
F_2	1032.57 ± 2.60	109.11 ± 0.29	0.9994	1228.04 ± 7.50	129.53 ± 0.82	0.9974	1167.84 ± 6.58	121.22 ± 0.71	0.9973
F_3	1223.12 ± 5.48	130.64 ± 0.61	0.9981	1492.57 ± 2.66	158.82 ± 0.29	0.9998	1393.79 ± 4.12	145.85 ± 0.44	0.9993
	β = 30°C/min			β = 40°C/min			β = 50°C/min		
Model	E_a (kJ/mol)	ln A (s^{-1})	r^2	E_a (kJ/mol)	ln A (s^{-1})	r^2	E_a (kJ/mol)	ln A (s^{-1})	r^2
$A_{3/2}$	597.75 ± 14.12	59.58 ± 1.51	0.9634	624.29 ± 14.94	62.15 ± 1.59	0.9641	587.15 ± 16.18	57.91 ± 1.70	0.9495
A_2	393.22 ± 12.86	37.68 ± 1.38	0.9321	418.60 ± 13.77	40.31 ± 1.47	0.9342	379.57 ± 14.78	36.05 ± 1.55	0.9039
A_3	188.70 ± 11.60	15.67 ± 1.24	0.7948	212.91 ± 12.61	18.35 ± 1.34	0.8139	172.00 ± 13.37	14.07 ± 1.41	0.7014
A_4	86.43 ± 10.98	4.58 ± 1.17	0.4729	110.06 ± 12.02	7.28 ± 1.28	0.5603	68.21 ± 12.67	3.00 ± 1.33	0.2856
R_1	735.60 ± 24.80	73.94 ± 2.65	0.9282	767.94 ± 25.72	77.01 ± 2.73	0.9320	724.85 ± 27.01	72.02 ± 2.84	0.9113
R_2	871.20 ± 20.71	87.88 ± 2.22	0.9630	901.80 ± 21.49	90.65 ± 2.28	0.9644	863.58 ± 23.00	86.05 ± 2.42	0.9527
R_3	916.40 ± 19.35	92.35 ± 2.07	0.9706	946.42 ± 20.08	95.02 ± 2.13	0.9716	909.82 ± 21.66	90.55 ± 2.28	0.9618
D_1	1833.61 ± 36.11	190.34 ± 3.86	0.9743	1874.49 ± 36.59	193.37 ± 3.88	0.9758	1838.24 ± 39.08	188.13 ± 4.11	0.9693
D_2	1962.76 ± 32.40	203.59 ± 3.47	0.9818	2002.08 ± 32.74	206.34 ± 3.47	0.9829	1970.31 ± 35.45	201.45 ± 3.73	0.9778
D_3	2099.08 ± 28.27	216.79 ± 3.02	0.9878	2136.64 ± 28.47	219.24 ± 3.02	0.9886	2109.78 ± 31.40	214.75 ± 3.30	0.9847
D_4	2008.68 ± 30.99	207.04 ± 3.32	0.9841	2047.40 ± 31.29	209.69 ± 3.32	0.9851	2017.29 ± 34.07	204.94 ± 3.58	0.9804
F_1	1006.80 ± 16.65	103.20 ± 1.78	0.9817	1035.67 ± 17.28	105.67 ± 1.83	0.9822	1002.30 ± 19.00	101.46 ± 2.00	0.9755
F_2	1278.01 ± 8.75	132.46 ± 0.94	0.9968	1303.40 ± 9.14	134.33 ± 0.97	0.9968	1279.75 ± 11.14	130.91 ± 1.17	0.9947
F_3	1549.21 ± 3.60	161.73 ± 0.39	0.9996	1571.13 ± 4.03	162.99 ± 0.43	0.9996	1557.20 ± 4.41	160.36 ± 0.46	0.9994

Levchnik,[27,28] as they are independent of the conversion, the model and the heating rate. The evaluation of the invariant activation parameters is performed from the supercorrelation:

$$\alpha_v^* = \ln A_{inv} - \beta_v^* E_{ainv} \tag{9}$$

The straight line, α_v* vs β_v*, allows us to determine the IKP (E_{ainv} and A_{inv}) from the slope and intercept.

It has been reported that the values of the invariant conversion function are proportional to their true values.[29,30] Therefore, the IKP method aims to determine the invariant parameters independent of the kinetic model; comparing the invariant parameters to those obtained using other methods also allows us to determine which kinetic model is better for describing the process.

(E) Master Plots: Recently, the as-known master plots are becoming increasing employed for the determination of the reaction models for solid-state reactions. The master plots are curves of the theoretical function of the reaction model and are independent of the Arrhenius parameters. The experimental kinetic data can easily be transformed into master plots, and the comparison between the theoretical and the experimental master plot leads to the selection of the appropriate reaction model, or at least, the appropriate type of kinetic model. There are two types of master plots: differential and integral. From Eqs. (3) and (4), for differential and integral plots, respectively, using a reference at point α = 0.5, the equations that are obtained are as follows:

$$\frac{f(\alpha)}{f(0.5)} = \frac{(d\alpha/d\theta)}{(d\alpha/d\theta)_{\alpha=0.5}} \tag{10}$$

$$\frac{g(\alpha)}{g(0.5)} = \frac{p(x)}{p(x_{0.5})} \tag{11}$$

where $p(x) = \frac{e^{-x}}{x}\pi(x)$; $p(x)$ has been obtained in the present article according to the Senum–Yang approximation.[31] The plot of $f(\alpha)/f(0.5)$ versus α corresponds to the differential theoretical master plot, and the plot of $g(\alpha)/g(0.5)$ versus α corresponds to the integral theoretical master plot (details can be found in Refs. 32 and 33). Information regarding the temperature as a function of α and the value of E_a must be known in advance to construct the experimental master plots for a given heating rate (additional explanation can be found in Refs. 32–36).

III. Results and Discussion

As previously mentioned, Teixeira *et al.*[12] have studied the crystallization of a wollastonite base glass using the Kissinger and Ligero methods.[37] In the present article, the same data from the original experiments have been reassessed, and E_a and ln A have been determined using several kinetic methods, specifically the isoconversional (KAS and Friedman) model fitting for a single, linear single heating rate, the IKR method employed under $f(\alpha)$, and heating rate variations, and the IKP method used with the integral and differential methods.

Once the E_{ainv} and ln A_{inv} parameters were obtained by using the IKP method, master plots were used to fit the experimental data using several functions of conversion.

(1) Isoconversional Methods

Figure 1 shows the variation of the activation energy with the degree of crystallization, (α). From this figure, it can be observed that the KAS and Friedman methods yield E_a values that are somewhat different over all α ranges, although they are on the same order of magnitude. These differences may be because the models are derived from different calculations of Eq. (2), as reported by other authors.[14] All E_a values determined from both methods exhibit standard errors lower than 10%. However, the results obtained using the Friedman method resulted in larger errors than those from the KAS method, as the way E_a is obtained from the Friedman method is more sensitive to noise from DTA thermograms.[36] The shapes of the E_a curves depicted from the two models are rather different, which could indicate the existence of more than one crystallization mechanism that fits the experimental results.

For the KAS method, the E_a values are approximately constant for α = 0.15–0.80, whereas for the Friedman method, E_a can be considered constant in the range of 0.1–0.45. Nevertheless, the curves in Fig. 1 exhibit a similar trend. The first part, where E_a is constant, indicates that crystallization occurs through a single mechanism; then, the change in E_a with increasing α reveals that the crystallization reaction changes to a multiple-step mechanism. The mean activation energy values that are determined in the intervals where E_a is constant are E_{aKAS} = 357 ± 6 kJ/mol and $E_{aFriedman}$ = 386 ± 5 kJ/mol. Both values are in agreement with those reported by Teixeira *et al.*[12] from application of the Kissinger and Ligero methods (374 and 378 kJ/mol).

It is shown in Fig. 1 that E_a is independent of the degree of crystallization in the range of 0.15–0.80 for the KAS and 0.05–0.45 for the Friedman methods. Model fitting, IKR, and IKP have been applied across those intervals.

(2) Model Fitting Methods

Tables I and II provide the results after application of the integral C–R [Eq. (6)] and the differential (*D*) [Eq. (7)] methods, respectively. It can be observed that a wide variety of results depend on the applied mechanism. If the collected E_a values shown in Tables I and II are compared with those determined previously using the isoconversional methods (357 and 386 kJ/mol), the function that yields a better fit to the experimental results corresponds to the Avrami mechanism, A_2, for both the C–R and D methods. Nevertheless, the E_a values that were determined from the DTA thermograms using different heating rates vary noticeably, which indicates that the wollastonite crystallization process cannot be adjusted to any of the mechanisms shown in Tables I and II. Therefore, these results suggest that there should be a more complex mechanism for the explanation of the crystallization process.

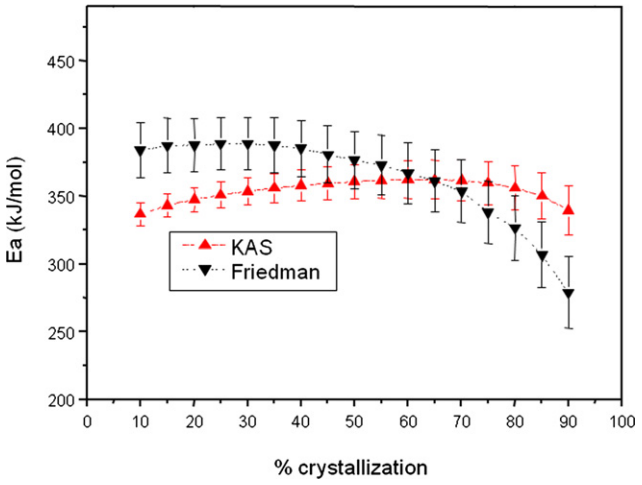

Fig. 1. Variation of activation energy with crystallization degree obtained by Friedman and KAS isoconversional methods.

(3) IKR Method

Tables III and IV show the correlation parameters from applying Eq. (8) to each mechanism for all heating rates. As previously explained, the values of T_{iso} can be obtained from the slope, β*. The most appropriate mechanism for the explanation of the crystallization process will be the one whose T_{iso} was within the devitrification experimental range as shown from the original DTA thermogram (800°C–950°C). In addition, the fit must have a good regression coefficient ($R^2 > 0.9$) using the proposed mechanism.[14,25] The integral results (Table III) show that the temperatures, T_{iso}, for the $A_{3/2}$, A_2, R_n, and F_n mechanisms are in the same range as experimental results; therefore, there is more than one mechanism that can fit the crystallization process. In the case of differential values (Table IV), the mechanisms that best fit T_{iso} are A_n. These results also confirm that the crystallization occurs through a complex mechanism.

Table III. Integral Isokinetic Parameters Determined from Eq. (8) for Different Reaction Mechanisms

Model	α* (min^{-1})	β* (mol/kJ)	r^2	T_{iso} (°C)
$A_{3/2}$	−2.8416 ± 3.3063	0.1114 ± 0.0068	0.9817	806.5
A_2	−2.5033 ± 0.7012	0.1119 ± 0.0019	0.9985	802.0
A_3	−2.2251 ± 2.1596	0.1125 ± 0.0092	0.9673	795.8
A_4	−2.1193 ± 3.3575	0.1128 ± 0.0197	0.8647	792.9
R_1	−0.9180 ± 3.8588	0.1068 ± 0.0075	0.9757	853.3
R_2	0.6546 ± 5.8856	0.1036 ± 0.0096	0.9586	887.6
R_3	1.1205 ± 6.5832	0.1026 ± 0.0101	0.9533	898.8
D_1	6.6228 ± 16.7912	0.0994 ± 0.0161	0.8819	936.9
D_2	9.0797 ± 19.0171	0.0977 ± 0.0163	0.8755	957.4
D_3	11.4652 ± 21.4915	0.0961 ± 0.0163	0.8714	978.6
D_4	8.8737 ± 19.8477	0.0971 ± 0.0163	0.8739	965.0
F_1	4.1205 ± 8.0102	0.1008 ± 0.0110	0.9436	920.2
F_2	1.0560 ± 2.0367	0.1058 ± 0.0042	0.9922	863.7
F_3	12.3848 ± 9.3041	0.0962 ± 0.0094	0.9540	976.7

Table IV. Differential Isokinetic Parameters Determined from Eq. (8) for Different Reaction Mechanisms

Model	α* (min^{-1})	β* (mol/kJ)	r^2	T_{iso} (°C)
$A_{3/2}$	−6.4436 ± 0.8699	0.1107 ± 0.0013	0.9994	813.4
A_2	−4.2251 ± 0.6018	0.1063 ± 0.0015	0.9990	858.2
A_3	−4.0816 ± 1.2098	0.1035 ± 0.0060	0.9837	888.5
A_4	−4.3957 ± 0.7539	0.1012 ± 0.0067	0.9786	915.0
R_1	6.0225 ± 4.0315	0.0922 ± 0.0056	0.9816	1032.1
R_2	7.5432 ± 4.7039	0.0920 ± 0.0056	0.9818	1034.5
R_3	7.7268 ± 4.9480	0.0921 ± 0.0056	0.9818	1032.8
D_1	20.5662 ± 11.3857	0.0924 ± 0.0065	0.9757	1028.4
D_2	21.2722 ± 12.0472	0.0927 ± 0.0065	0.9763	1024.2
D_3	21.2478 ± 12.7430	0.0930 ± 0.0064	0.9768	1020.5
D_4	20.2632 ± 12.2805	0.0928 ± 0.0064	0.9765	1022.9
F_1	9.9191 ± 5.4452	0.0924 ± 0.0056	0.9817	1028.5
F_2	12.9976 ± 6.9401	0.0932 ± 0.0057	0.9816	1017.0
F_3	16.0591 ± 8.4151	0.0938 ± 0.0057	0.9816	1009.4

Table V. Values of Integral and Differential Compensation Parameters Calculated from Data in Tables I and II

	Integral				Differential			
β (°C/min)	α* (min^{-1})	β* (mol/kJ)	T_{iso} (°C)	r^2	α* (min^{-1})	β* (mol/kJ)	T_i (°C)	r^2
5	−1.5752 ± 0.7013	0.1093 ± 0.0009	827	0.9991	−5.6905 ± 0.5156	0.1100 ± 0.0005	821	0.9997
10	−0.8423 ± 0.7175	0.1078 ± 0.0009	843	0.9992	−4.9631 ± 0.4694	0.1085 ± 0.0004	836	0.9998
20	−0.3125 ± 0.7163	0.1057 ± 0.0010	865	0.9989	−4.1696 ± 0.6798	0.1064 ± 0.0006	857	0.9996
30	0.1546 ± 0.7240	0.1050 ± 0.0009	872	0.9991	−3.8704 ± 0.4805	0.1057 ± 0.0004	865	0.9998
40	0.4258 ± 0.7259	0.1042 ± 0.0009	882	0.9991	−3.5644 ± 0.4858	0.1048 ± 0.0004	874	0.9998
50	0.6132 ± 0.7240	0.1032 ± 0.0009	892	0.9990	−3.4066 ± 0.4753	0.1040 ± 0.0004	884	0.9998

Table V shows the integral and differential compensation parameters determined from applying Eq. (8) to the data in Tables I and II. At each heating rate, the mechanisms that resulted in better fits to the experimental results have been considered for calculations. In this case, all the T_{iso} values are within the experimental wollastonite crystallization range, and furthermore, the regressions are better than those presented in Tables III and IV.

Taking the data collected in Tables III–V into account, it can be observed that the IKR method is unable to establish an appropriate model for this crystallization process.

(4) IKP Method

The IKP obtained from Table V by applying Eq. (9) are E_{ainv} = 386 ± 20 kJ/mol and ln A_{inv} = 37 ± 2 for the differential model and E_{ainv} = 362 ± 23 kJ/mol and ln A_{inv} = 38 ± 2 for the integral model. It can be seen that both E_{ainv} and ln A_{inv} determined from the integral and differential models are similar.

The E_{ainv} and ln A_{inv} values are in agreement with those reported in the previous paper[12] and are also similar to the values calculated for model A_2 (Tables I and II).

(5) Master Plots

Master plots that have been drawn to verify the model, or models, result in better fits to the experimental results. Figure 2 shows the results of the differential master plot from the application of Eq. (10). The theoretical curves drawn ($A_{3/2}$, A_2, and F_1) are those that yielded the best fits to experimental data. For degrees of crystallization lower than 0.5, the experimental curve depicts a trend similar to the Avrami ($A_{3/2}$ and A_2) theoretical curves, whereas at higher conversion degrees, the mechanism that yield the best fit is F_1, which indicates a first-order reaction that is coincident with the Avrami mechanism for surface crystallization. These results disagree with those previously obtained using the isoconversional Friedman method. In Fig. 1, the E_a determined from the Friedman method is constant in the range of 0.05–0.45, whereas the master plot (Fig. 2) shows an unfitted Avrami-like mechanism. For α > 0.45, the F_1 mechanism results in a better fit in the master plot, but Fig. 1 shows that this range corresponds to a multiple-step mechanism. Therefore, the wollastonite crystallization mechanism cannot be obtained by applying the Friedman method and differential master plot together.

Figure 3 presents the integral master plot obtained by applying Eq. (11). Similar to Fig. 2, only the theoretical curves that resulted in better fits ($A_{3/2}$, A_2, A_3, and F_1)) are shown along with the experimental results. In this case, the theoretical curve that corresponds to A_3 mechanism is best fitted in the α = 0.05–0.4 interval, whereas from 0.4 to 0.8, the crystallization is adjusted for the $A_{3/2}$ mechanism. These results indicate a complex mechanism of three-dimensional growth of crystals with a constant number of nuclei (A_3) in the surface of the glass particles, and subsequently volume crystallization, originated from the one-dimensional growth of needles by diffusion control ($A_{3/2}$) from the surface to the interior of glass particles.

As final remark, it can be said that the kinetic methods applied in this study indicate a complex crystallization mechanism that agrees with the results previously reported by Teixeira *et al.*[12] i.e., the initial development of a crystallization shell that is composed of spherulitic crystal (three-dimensional) followed by the growth of linear fiber-like crystals into the glass sample.

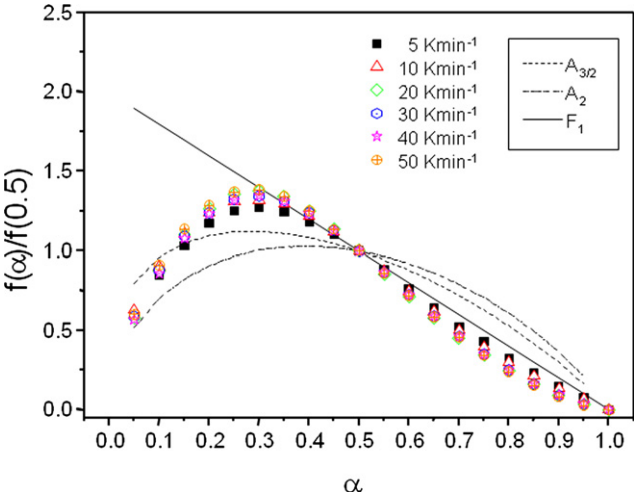

Fig. 2. Theoretical (lines) differential master plots of $f(\alpha)/f(0.5)$ vs α and the experimental master curve (symbols).

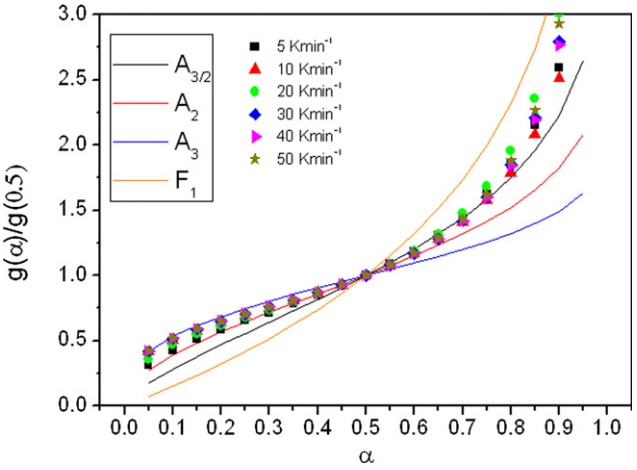

Fig. 3. Theoretical (lines) integral master plots of $g(\alpha)/g(0.5)$ vs α and the experimental master curve (symbols).

IV. Conclusions

The complex crystallization mechanism of a wollastonite glass has been established from a non-isothermal kinetic study by means of DTA. This study has allowed the determination of the activation energy (E_a), pre-exponential factor (A) and, when possible, the function of conversion ($f(\alpha)$). To assess the crystallization mechanism (single and/or multiple steps), both the integral KAS method and the differential Friedman isoconversional methods were used. The isokinetic temperature (T_{iso}) was determined from the IKR, whereas the Isokinetic Parameters method was used to obtain both the invariant activation energy (E_{ainv}) and the pre-exponential factor (A_{inv}). To determine the $f(\alpha)$, the Master Plots (differential and integral) were applied.

The activation energies, which were determined using the isoconversional methods, are in range 360–386 kJ/mol. These values agree with the IKP, which were obtained from the application of both integral (E_{ainv} = 362 kJ/mol) and differential (E_{ainv} = 386 kJ/mol) methods.

Isoconversional methods have revealed that the crystallization process occurs in two stages, a first step that has constant activation energy (single step mechanism) followed by a later step that is characterized by the variation of activation energy with the conversional degree (multi-step mechanism).

Master plots indicate that the wollastonite crystallization takes place through a complex mechanism. In the α = 0.05–0.4 interval, the three-dimensional growth of crystals with a constant number of nuclei (A_3) occurs on the surface of the glass particles. Later, in the α = 0.4–0.8 interval, the crystallization is adjusted to the $A_{3/2}$ mechanism, which means that one-dimensional growth of needles occurs by diffusion control from the surface to the interior of glass particles.

Acknowledgments

One of the authors (J.M. Pérez) would like to acknowledge CSIC for the financial support by contract JAEDoc-08-00362. S.R. Teixeira is greatly indebted to FAPEST (04368-4/08 and to UNESP/PROPE-SANTANDER postdoc program for the scholarship.

References

[1]R. D. Rawlings, J. P. Wu, and A. R. Boccaccini, "Glass-Ceramics: Their Production from Wastes- A Review," *J. Mater. Sci.*, **41** [3] 733–61 (2006).

[2]W. Höland and G. Beall, *Glass-Ceramic Technology*. The American Ceramic Society, Westerville, OH, 2002.

[3]M. Romero and J. Ma. Rincón, "The Controlled Vitrification/Crystallisation Process Applied to the Recycling of Inorganic Industrial Wastes," *Bol. Soc. Esp. Ceram. Vid.*, **39** [1] 155–63 (2000).

[4]M. S. Hernandez-Crespo, M. Romero, and J. Ma. Rincón, "Nucleation and Crystal Growth of Glasses Produced by a Generic Plasma Arc-Process," *J. Eur. Ceram. Soc.*, **26** [9] 1679–85 (2006).

[5]M. Romero, M. S. Hernández-Crespo, and J. Ma. Rincón, "Leaching Behaviour of a Glassy Slag and Derived Glass Ceramics from Arc Plasma Vitrification of Hospital Wastes," *Adv. Appl. Ceram.*, **108** [1] 67–71 (2009).

[6]L. Barbieri, I. Lancellotti, T. Manfredini, G. C. Pellacani, J. Ma. Rincón, and M. Romero, "Nucleation and Crystallization of New Glasses from Fly Ash Originating from Thermal Power Plants," *J. Am. Ceram. Soc.*, **84** [8] 1851–8 (2001).

[7]M. Romero, M. Kovacova, and J. Ma. Rincón, "Effect of Particle Size on Kinetics Crystallization of an Iron-Rich Glass," *J. Mater. Sci.*, **43** [12] 4135–42 (2008).

[8]F. A. López, M. I. Martín, F. J. Alguacil, J. Ma. Rincón, T. A. Centeno, and M. Romero, "Thermolysis of Fibreglass Polyester Composite and Reutilisation of the Glass Fibre Residue to Obtain a Glass–Ceramic Material," *J. Anal. Appl. Pyrol.*, **93** [1] 104–12 (2012).

[9]M. I. Martín, J. Ma. Rincón, F. Andreola, L. Barbieri, I. Lancellotti, and M. Romero, "Materiales Vitrocerámicos del Sistema MgO-Al_2O_3-SiO_2 a Partir de Ceniza de Cáscara de Arroz," *Bol. Soc. Esp. Ceram. Vid.*, **50** [4] 201–6 (2011).

[10]J. Ma. Rincón, "Principles of Nucleation and Controlled Crystallisation of Glasses," *Polym. Plast. Technol. Eng.*, **31** [3–4] 309–57 (1992).

[11]M. Romero, R. D. Rawlings, and J. Ma. Rincón, "Crystal Nucleation and Growth in Glasses from Inorganic Wastes from Urban Incineration," *J. Non-Cryst. Solids*, **271** [1–2] 106–18 (2000).

[12]S. R. Teixeira, M. Romero, and J. Ma. Rincón, "Crystallization of SiO_2-CaO-Na_2O Glass Using Sugarcane Bagasse Ash as Silica Source," *J. Am. Ceram. Soc.*, **93** [2] 450–5 (2010).

[13]A. Rotaru, A. Moanta, I. Sălăgeanu, P. Budrugeac, and E. Segal, "Thermal Decomposition Kinetics of Some Aromatic Azomonoethers. Part I. Decomposition of 4-[(4-Chlorobenxyl)oxy]-4′-Nitro-Azobenzene," *J. Therm. Anal. Calorim.*, **87** [2] 395–400 (2007).

[14]A. Cadenato, J. M. Morancho, X. Fernández-Francos, J. M. Salla, and X. Ramis, "Comparative Kinetic Study of the Non-Isothermal Thermal Curing of Bis-GMA/TEGDMA Systems," *J. Them. Anal. Calorim.*, **89** [1] 233–44 (2007).

[15]X. Ramis, J. M. Salla, and J. Puiggalí, "Kinetic Studies on the Thermal Polymerization of N-Chloroacetyl-11-Aminoundecanoate Potassium Salt," *J. Polym. Sci. Part A*, **43** [6] 1166–76 (2005).

[16]B. Janković, B. Adnadevic, and S. Mentus, "The Kinetic Analysis of Non-Isothermal Nickel Oxide Reduction in Hydrogen Atmosphere Using the Invariant Kinetic Parameters Method," *Thermochim. Acta*, **456** [1] 48–55 (2007).

[17]O. C. Mocioiu, M. Zaharescu, G. Jitianu, and P. Budrugeac, "Kinetic Parameters Determination in Non-Isothermal Conditions for the Crystallization of A Silica-Soda-Lead Glass," *J. Therm. Anal. Calorim.*, **86** [2] 429–36 (2006).

[18]J. M. Pérez, J. M. Rincón, and Ma. Romero, "Study of Mullite Formation in Porcelain Stoneware Applying Isoconversional and IKP Methods," *Ceram. Int.*, **36** [8] 2329–35 (2010).

[19]H. L. Friedman, "Kinetics of Thermal Degradation of Char-Forming Plastics from Thermogravimetry. Application to a Phenolic Plastic," *J. Polym. Sci. Part C*, **6** [1] 183–95 (1964).

[20]H. E. Kissinger, "Reaction Kinetics in Differential Thermal Analysis," *Anal. Chem.*, **29** [11] 1702–6 (1957).

[21]T. Akahira and T. Sunose, "Joint Convention of Four Electrical Institutes," *Res. Report Chiba. Inst. Technol.*, **16**, 22–31 (1971).

[22]C. D. Doyle, "Estimating Thermal Stability of Experimental Polymers by Empirical Thermogravimetric Analysis," *Anal. Chem.*, **33** [1] 77–9 (1961).

[23]P. Murray and J. White, "Kinetics of the Thermal De-Hydration of Clays," *Trans. Br. Ceram. Soc.*, **54**, 151–87 (1955).

[24]A. W. Coats and J. P. Redfern, "Kinetics Parameters from Thermogravimetric Data," *Nature*, **201**, 68–9 (1964).

[25]S. Vyazovkin and W. Linert, "False Isokinetic Relationships Found in the Nonisothermal Decomposition of Solids," *Chem. Phys.*, **193** [1] 109–18 (1995).

[26]S. Vyazovkin and W. Linert, "The Application of Isoconversional Methods for Analyzing Isokinetic Relationships Occurring at Thermal Decomposition of Solids," *J. Solid State Chem.*, **114** [2] 392–8 (1995).

[27]A. I. Lesnikovich and S. V. Levchik, "A Method of Finding Invariant Values of Kinetic Parameters," *J. Therm. Anal. Calorim.*, **27** [1] 89–94 (1983).

[28]A. I. Lesnikovich and S. V. Levchik, "Isoparametric Kinetic Relationship for Chemical Transformations in Condensed Substances (Analytical Survey). II. Reactions Involving the Participation of Solids Substances," *J. Therm. Anal. Calorim.*, **30** [3] 667–702 (1985).

[29]P. Budrugeac, "Some Methodological Problems Concerning the Kinetic Analysis of Non-Isothermal Data for Thermal and Thermo-Oxidative Degradation of Polymers and Polymeric Materials," *Polym. Degrad. Stab.*, **89** [2] 265–73 (2005).

[30]P. Budrugeac and E. Segal, "On the Kinetic Processing of Thermal Analysis Data," *Rev. Roum. Chim.*, **49** [3–4] 193–8 (2004).

[31]G. I. Senum and R. T. Yang, "Rational Approximations of the Integral of the Arrhenius Function," *J. Therm. Anal. Calorim.*, **11** [3] 445–7 (1977).

[32]F. J. Gotor, J. M. Criado, J. Malek, and N. Koga, "Kinetic Analysis of Solid-State Reactions: The Universality of Master Plots for Analysing Isothermal and Nonisothermal Experiments," *J. Phys. Chem. A*, **104** [46] 10777–82 (2000).

[33]J. M. Criado, L. A. Pérez-Maqueda, F. J. Gotor, J. Malek, and N. Koga, "A Unified Theory for the Kinetic Analysis of Solid State Reactions Under Any Thermal Pathway," *J. Therm. Anal. Calorim.*, **72** [3] 901–6 (2003).

[34]J. M. Morancho, A. Cadenato, X. Fernández-Francos, J. M. Salla, and X. Ramis, "Isothermal Kinetics of Photopolymerization and Thermal Polymerization of bis-GMA/TEGDMA Resins," *J. Therm. Anal. Calorim.*, **92** [2] 513–22 (2008).

[35]B. Janković, B. Adnadević, and J. Jovanović, "Application of Model-Fitting ad Model –Free Kinetics to the Study of Non-Isothermal Dehydration of Equilibrium Swollen Poly (Acrylic Acid) Hydrogel: Thermogravimetric Analysis," *Thermochim. Acta*, **452** [2] 106–15 (2007).

[36]S. Vyazovkin, A. K. Burham, J. M. Criado, L. A. Perez-Maqueda, C. Popescu, and N. Sbirrazzuolli, "ICTAC Kinetics Committee Recommendations for Performing Kinetic Computations on Thermal Analysis Data," *Thermochim. Acta*, **520** [1–2] 1–19 (2011).

[37]R. A. Ligero, J. Vázquez, M. Casa-Ruiz, and R. Jiménez-Garay, "A Study of the Crystallization Kinetics of Some Cu-As-Te Glasses," *J. Mater. Sci.*, **26** [1] 211–5 (1991). □